Synthesis and Characterization of Turmeric Powered Bio-Significant 'Organometallic Aluminates'

Vishnu Prabhakar*, Rupesh Kumar, Aditi
Nanotechnology research center, DAVIET, Jalandhar, 144008 India

Research Article

Article Info
Recived on:10/02/2015
Accepted on: 17/02/2015
Published on: 20/02/2015

QR Code for mobile

Literati Open Access

ABSTRACT :

Nanohybrid organometallic particles of 'C-γ-alumina' and 'C-α-alumina' have been synthesized through thermal decomposition method. Simultaneous propulsion of organic herb turmeric and inorganic aluminum nitrate on temperature 700°C disclosed formative ability within turmeric molecules that wisely derived a covalent-ionic bonded prominent self-assembled structure of C-γ-alumina in an uncontrolled environment. Turmeric transformed alkaloid carbon derivatives provoked activation in nano C-γ-alumina. In-vitro elaboration of minimal inhibitory concentration (MIC) against pathogenic strain *Acinetobactor* Sp. and, *ex-situ* TDS measurement of contaminated water further showed enhance biochemical efficacy of C-γ-alumina nanoparticles in different surrounding environments. Phase transition of C-γ-alumina into more thermodynamically stable C-α-alumina retained on temperature 700°C during a second thermal decomposition propelled by fuel hexamine. Occurrence of a single C-O carbonyl bond in FTIR absorption spectra, obtained for both carbon aluminates latter verified organometallic nature of compounds. Phase transition characteristics, crystalline size and crystalline phases were determined by X-Ray diffraction. High resolution TEM and FESEM imaging's displayed spherical surface morphology of C-γ-alumina and captured rough surface features in transformed C-α-alumina at down to the nanoscale.

Keywords: Organometallic chemistry, electronegativity, self-assembly, phase transition, hexamine.

INTRODUCTION:

Engineered alumina or aluminum oxide (Al_2O_3), in raw form of bauxite is the most versatile mineral produced by abditory nature that has remained faithful for humans as bioimplant material since 1975 [1]. This mineral is widely accepted ceramic biomaterial for the excellent properties it offers. High elastic modulus (~380GPa), hardness (28GPa), melting point (2070°C) [2-4] together with biocompatibility [5] of alumina has remarkably proven its significance in fabrication of artificial hip-knee joints, dental and bone spacer plates [6-7]. In more general field of medical science alumina ceramic also has been used to manufacture homeopathy medicines, blood transfusion membranes, medicinal potteries and other scientific products [8-9]. Though alumina is reliable, biocompatible and biostable ceramic, a histologically proven set of unexpected biological loosening's (osteolysis) [10] in alumina implants has been originated by one of its own superb property i.e. bio-chemical 'inertness' [10], which subsequently reduced its degree of popularity in direct blood-bones contacting implant and scaffold materials [11]. In consolidated implant failure investigations, several of alumina implants showed extreme inertness and were failed to encourage bone growth (ossification) [12] due to insignificant biological bonding (interfacial interaction, tissue adhesion and cell migration) [13] was drawn by host tissues around the ultrastructure boundary of bone-implant. In past decades alumina has been doped with various inorganic materials like calcium, zirconium, magnesium, and chromium to enhance biochemical properties of bioimplants but they were most likely to be subject of cracks and dynamic fatigue [14-16]

doi: 10.15272/ajbps.v5i41.669

**Corresponding author:*
Vishnu Prabhakar
Nanotechnology research center, DAVIET, Jalandhar, 144008 India , Email: vaashu.bme@gmail.com,
Tel: +919450247989
Conflict of interest: Authors reported none

generation. A common secondary problem associated with alumina is the low temperature synthesis of thermodynamically stable α-alumina phase [17] which requires high temperature of over ~1100°C [18] to gain hexagonal closest-packed (hcp) structure. Cava *et al*. (2007) [19] obtained the lowest synthesis temperature 1025°C on which α-alumina nanoparticles synthesized through polymeric precursor method. In another work, phase transformation of flame synthesized gamma (γ)-alumina to alpha (α)-alumina on temperature 1200°C was examined by Gyo Lee *et al.* (2013) [20]. The overall reviews on alumina indicates; a necessity to increase bio-functionality of metastable alumina together with low temperature growth of alpha (α) phase, to make alumina more meaningful biomaterial.

Present work proclaimed on marvelous capabilities of Mother Nature's parallel strengthening the overall biochemical and physical properties of alumina through introduction of carbon. Thamaraiselvi *et al.* (2004) [1] emphasized excellent biocompatibility and mechanical properties of carbon similar to bones, thus indicates carbon can be deploy as a biomaterial particularly in blood contact orthopedic implants. Natural spice turmeric (Curcuma longa) is well known to contain curcuminoids, a compound believed to have anticancer effects [21], and when burnt into carbon simultaneously with aluminum nitrate on temperature 700°C, ends-up into covalent-ionic bonded organometallic C-γ-alumina (C-γ-AlO_2). Nanohybrid semi-crystalline grains of C-γ-alumina with fused grain boundaries at nanoscale have potential to compete with current medical grade alumina having grain size 1.4 μm [3], while lower surface energy of γ-alumina ensured availability of larger active surface area for catalytic reactions. Moreover, to obtain low temperature α-alumina phase, present work dealt with phase transition of C-γ-alumina into more thermodynamically stable, polycrystalline C-α-alumina (C-α-Al_2O_3) at temperature down to 700°C by introducing hexamine propellant in thermal decomposition of alumina.

MATERIALS AND METHODOLOGY:

Formations of desired organometallic frameworks (C-γ-alumina, C-α-alumina) obtained by high temperature thermal decomposition of solution based constituent precursors in two stages, propelled by two distinct fuels. In first stage, to synthesize C-γ-alumina; 3.75gm salt of analytical grade aluminium nitrate [$Al(NO_3)_3.9H_2O$ (Nice Chem.)] and 2.88gm of propellant urea [NH_2CONH_2 (CDH Ltd.)] were dissolved in 8ml of distilled water. Intimate blending of 0.55gm fine turmeric powder (Alleppey Finger) in redox solution of fuel and metal nitrate served a delicate source of carbon. 100ml silica crucible was used as an ignition pot due to withstand capability of silica on higher temperature. At room temperature solution was kept in rest condition (without stirring) for 20 minutes, showed change in color of redox solution from transparent into dark brown with essence of golden color, further confirmed the reactive properties of turmeric molecules. Initially, the solution was preheated upon a hot plate on temperature 300°C with continuous stirring till half of the water evaporated and solution homogenized well. Resultant redox solution when introduced into 700°C preheated muffle furnace, burnt in suppressed manner. A gentle pyrolytic decomposition of redox solution into carbonized foam of C-γ-alumina was arrived at completion in less than 4 minutes. Evolution of moderately acute by-product gases prevented unnecessary sintering as well as dissipated the heat of combustion. After 2 hours of calcination on the same temperature was used for ignition, foam was then cooled down and lightly grounded in agate mortar to obtain fine nanoparticles of C-γ-alumina.

The purpose of second thermal decomposition using hexamine fuel was to confirm the parent material i.e. what carbon hiding within it? Its aluminum oxide or pure metal aluminum in previously made C-γ-alumina, followed by low temperature growth of α-alumina. Experimental procedure began with the removal of carbon from C-γ-alumina. For this, 2gm of as-synthesized C-γ-alumina nanoparticles (fig. 1a) were refluxed in 6 moles of concentrated nitric acid with continuous stirring upon a hot plate on temperature 300°C. Formation of dark black solution (fig. 1b) through nitric acid confirmed the removal of carbon from C-γ-alumina. A second solution of fuel contained 1.8gm of hexamine [$C_6H_{12}N_4$ (Lobachemie.)] dissolved in 8ml of distilled water was then added into carbon rich solution through vigorous stirring on temperature 150°C. Resultant homogeneous solution when introduced into preheated muffle furnace at temperature 700°C explosively decomposed (fig. 1c) into pure white (fig. 1d) agglomerates of α-alumina. During combustion with hexamine excessive energetic flames were observed for a prolonged period of time. Ignition temperature helped in crystallization, whereas extended decomposition time adversely transformed C-γ-alumina into polycrystalline α-alumina at temperature down to 700°C. Mild presence of carbon in α-alumina crystal lattice latter verified by XRD and FTIR spectrums, displayed an organometallic-polycrystalline alpha aluminate (C-α-alumina). The overall thermal decomposition process followed

the rules of propellant chemistry that can be more exothermic or explosive for improper fuel to oxidizer ratio so it is suggested to wear proper protecting gears and should be undertaken with extra precautions.

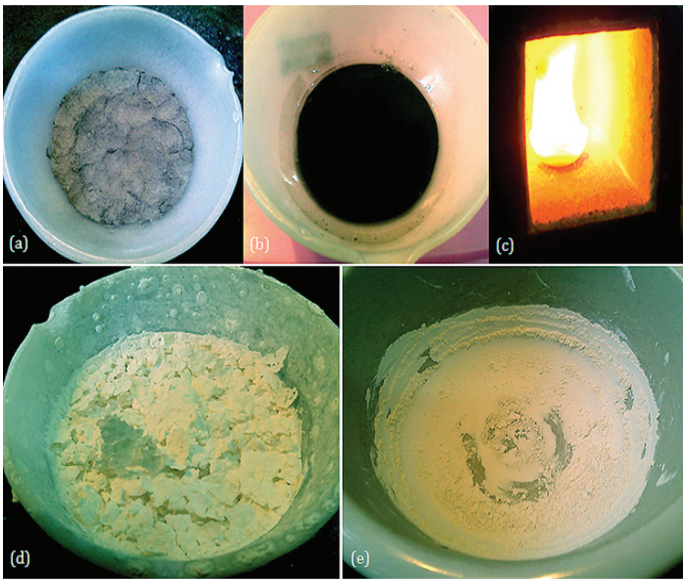

Figure 1. Phase transition sequence of C-γ-alumina into polycrystalline C-α-alumina; (a) gray color of C-γ-alumina nanoparticles confirmed the presence of carbon, (b) removal of carbon through nitric acid, (c) propulsion of carbon rich black solution with fuel hexamine on temperature 700°C, (d) Hard agglomerates of polycrystalline C-α-alumina after explosive decomposition, (e) nanoparticles of C-α-alumina after 2 hours grinding in mortar.

CHARACTERIZATION:

Crystalline size and crystalline phases of organometallic specimens were evaluated by "Philips diffractometer" (PANalytical X'Pert Pro, PW 3050/60 with CuKα=1.5406Å radiation generated at 40kV and 40mA) equipped with a fixed 100mm focused divergence slit. The specimens were measured in the 2θ range of 10°-90° with scan step of 0.017° in 20 seconds of scanning time at room temperature. Silicon was used to correct instrumental broadening. A combination of transmission and scanning electron microscopes was employed for morphological imaging of specimens on nanoscale. TEM images were captured by using 'TECNAI G2 20 S-TWIN' (200kV) electron microscope inbuilt with 'Gatan SC-200D Orius' and 'Gatan 894 ultra-scan 1000' high resolution CCD cameras. Samples were prepared for TEM imaging by dipping and drying porous 3mm carbon coated copper grids into 20 minutes pre-ultrasonified methanolic dispersion of specimen powders. In parallel, SEM images were obtained by using ultra low vacuum (10-130Pa extended up to 4000Pa) operated 'FEI-Quanta 200 FESEM' electron microscope with accelerating voltage 20kV. Samples for SEM were prepared by direct gluing of specimen powders onto the surface of single stub which further placed on four axial motorized 'Stage' for characterization. FTIR spectrums of specimens were recorded in between 4000-450cm^{-1} absorbance range by using "Varian 1000 FTIR". The specimen powders were grounded with 200mg of potassium bromide (KBr) in agate mortar and latter compressed in hand press to obtain 10mm diameter pellets for FTIR analysis.

RESULT AND DISCUSSION:

Molecular self-assembly in biology is usually characterized by a spontaneous process under minimum thermodynamic equilibrium to generate non-covalently bonded higher order aggregates from relatively smaller subunits [22]. In contrast, organometallic chemistry relies strictly on covalent-ionic bonding of carbon with metals [23]. This is quite difficult to obtain self-assembly in organometallic compounds due to complexity of carbon to make stable bonds (single, double or triple) with dissimilar electronegative inorganic elements [24]. By present work, thermal decomposition through solution combustion signified its potential to fabricate self-assembled organometallic C-γ-alumina (C-γ-AlO_2), comprised of different electronegative elements. For example, carbon and oxygen often favored to establish polar-covalent bonds (C-O) with each other by their respective electronegativities 2.55 (C) and 3.44 (O) [24], whereas the aluminum ions (Al^{3+}) in salt of aluminum nitrate has secured minimum electronegativity 1.61 on Pauling scale [25]. This huge differences in electronegativities of carbon and oxygen in comparison with aluminum when combined, furnished a 'covalent-ionic' [25] framework within C-γ-alumina. Elevated temperature 700°C forcedly helped to push covalent carbon atoms (turmeric transformed) into ionic γ-alumina crystal lattice.

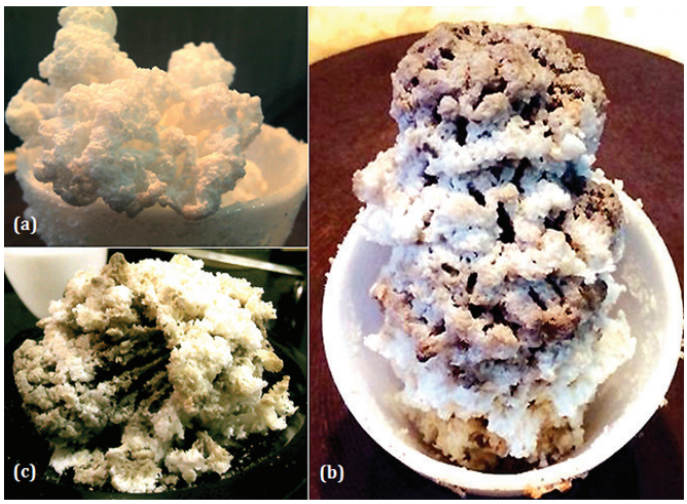

Figure 2. Random structure (a) of θ alumina, in comparison with well self-assembled structure (b) of C-γ-alumina supported by hyper branched (c) flower like interior after thermal decomposition.

Parallel significance of temperature, combustion with turmeric molecules manifested "Heat

assisted covalent-ionic self-assembly" a quite new phenomenon, mimicked the concept of biological self-assembly to direct a spontaneous, three dimensional prominent structure of C-γ-alumina (fig. 2b) in a well-defined connectivity and shape. The observed plausibility of self-assembled C-γ-alumina was knitted intentionally by turmeric molecules, which performed their function as a biological catalyst encoded with formative biological information (same as human genes) to target structure of a specific topology. This prodigious structure targeting ability of turmeric molecules unveiled hidden secrets of Mother Nature's and remained facsimile in several trials. The identical cage patterns in bulk C-γ-alumina followed the clockwise rotational patterns of gray and bright white colors respectively. Hyper branched isotropic interior skeleton (fig. 2c) served as an extension to hold exterior framework of self-assembled C-γ-alumina. Moreover, the low temperature (700°C) irreversible phase transformation of C-γ-alumina into more thermodynamically stable C-α-alumina during second thermal decomposition signified the profound impact of propellant hexamine in determination of material characteristics. This dramatic reduction in growth temperature from ~1100°C (standard condition for α-alumina) to 700°C further confirmed by X-Ray diffraction and was achieved by two main factors; (i) a platform (i.e. γ-alumina) for initial nucleation of α-alumina was provided by the first thermal decomposition with fuel urea and (ii) nucleation growth ends-up with desired α-alumina phase by prolonged violent flames, explosively produced by nitrogen rich fuel hexamine during second decomposition. It has been concluded that the low temperature α-alumina growth is feasible by controlling the primary nucleation step as well as by choosing propellant with extended aerial burning time.

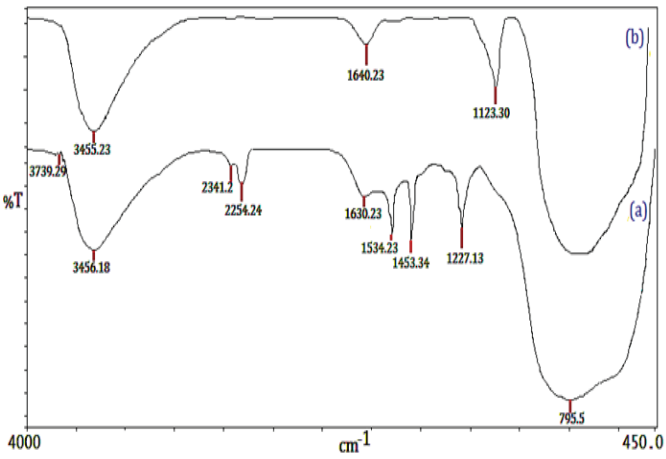

Figure 3. FTIR spectrums (a) obtained for rich in functional groups C-γ-alumina and, (b) elimination of functional groups in transformed C-α-alumina.

After grinding of as-synthesized specimens, FTIR spectroscopy confirmed the inclusion of various functional groups within nano C-γ-alumina (fig. 3a), most specially, at point 3739.29cm^{-1} in high energy region of spectrum a phenol group exhibited due to the stretch free vibrations of hydroxyl ions (OH) present in phenol. Phenol is generally a compound of 'phenyl' bonded to OH, so that a cluster of sharp peaks at points 1534.23cm^{-1} and 1453.34cm^{-1} also obtained by stretching vibrations of aromatic phenyl rings [26]. A single bending vibration of aromatic phenyl rings was generated at point 795.5cm^{-1}. Another OH ion stretching vibration band at point 3456.18cm^{-1} observed along with its second adsorptive bending vibration at point 1630.23cm^{-1} indicates, moisture in specimen and usually caused by water absorption during the preparation of C-γ-alumina pellet with potassium bromide (KBr). The week symmetrical stretches at points 2341.25cm^{-1} and 2254.24cm^{-1} signified a monovalent multiple bonded aliphatic cyanide/nitrile (-C≡N) compound [26]. Formation of γ-alumina phase with single C-O bond was characterized by an intense peak of carbonyl group at point 1227.13cm^{-1} [27] thus fulfilled the criteria to being an organometallic C-γ-alumina. In contrast, IR spectrum for transformed α-alumina (fig. 3b) confirmed the elimination of functional groups in second combustion with hexamine fuel, except that single C-O carbonyl bond shifted and signified a polycrystalline organometallic C-α-alumina at point 1123.30cm^{-1}.

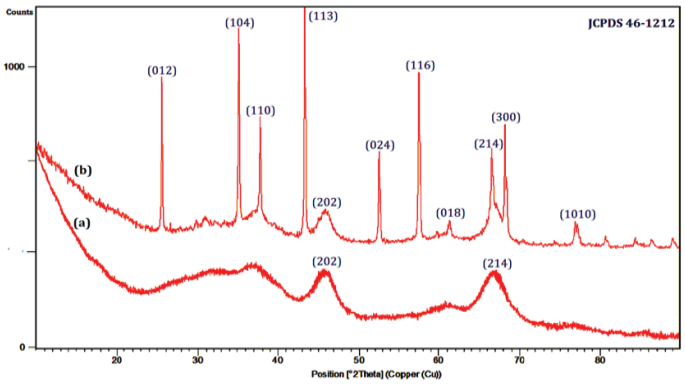

Figure 4. X-ray diffraction profile obtained for (a) randomly arranged crystal structure of C-γ-alumina and, (b) 700°C transformed polycrystalline C-α-alumina.

Evolution of organometallic frameworks also confirmed by X-Ray diffraction data, illustrated atomic scale mixing of carbon with γ and α alumina phases. All obtained crystalline planes were arranged by their respective d-spacing and matched exactly with standard JCPDS card 46-1212 for alumina. Average primary particle size 25.75nm for C-γ-alumina, and 83.82nm for C-α-alumina were calculated by using Sherrer's equation [28] i.e.

$$t = (K\lambda)/(\beta \cos\theta)$$

Where, K is the Scherrer constant with value 0.89, λ

is the wavelength of X-Ray radiation, β is full width at half maxima (FWHM) of the Bragg peak in radians, θ is the Bragg angel of diffracted peak. Initial XRD profile (fig. 4a) obtained for organometallic C-γ-alumina specimen synthesized on typical temperature 700°C. Elevated temperature fulfilled the stoichiometric of combustion reaction and thermally decomposed starting precursor materials into less crystalline metastable C-γ-alumina. Presence of only two crystalline planes 202 and 214 indicates low degree periodicity or random distribution of atoms within C-γ-alumina crystal lattice. Broader widths of diffraction peaks were results of poor planar reflections of X-Ray beams produced by poorly arranged crystal unit cells, which further developed inverse relationship with FWHM (full width at half maximum) to ensure smaller size nanoparticles (26.75nm). The linkage between carbon and alumina was identified by a strong zigzag scattering profile (turbulence) fused in diffraction base line denoted a hybrid, semi-crystalline lattice comprised of carbon rich amorphous and γ-alumina crystalline phases (i.e. C-γ-alumina). Second XRD profile (fig. 4b) illustrates successful transformation of C-γ-alumina into more periodically arranged polycrystalline C-α-alumina that almost contained all crystalline planes (012), (104), (110), (113), (202), (024), (116), (018), (214), (300), (1010) of thermodynamically stable α-alumina within its crystal structure. Crystal planes were well defined by tall narrow peaks and matched exactly with JCPDS standard. In parallel with narrow and sharp peaks of α-alumina, carbon also signified itself by inducing mild scattering patterns in bottom of diffraction base line, thus overall profile indicates C-α-alumina was also an organometallic compound but poor in carbon (contained only single C-O carbonyl bond).

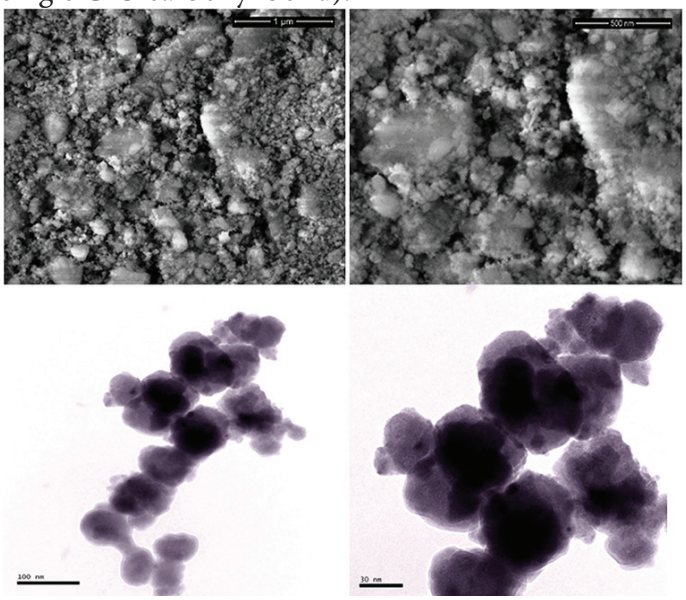

Figure 5. Porous low density SEM and TEM micrographs obtained for spherical C-γ-alumina nanoparticles.

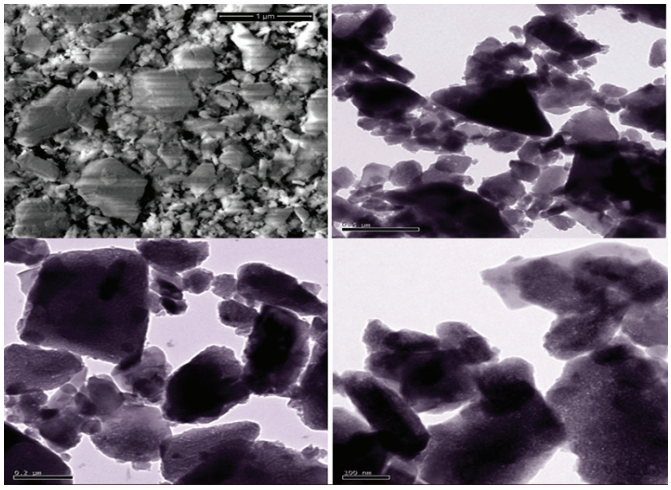

Figure 6. Platy-asymmetrical SEM and TEM micrographs obtained for C-γ-alumina transformed C-α-alumina nanoparticles.

Morphological characterizations examined through SEM and TEM imaging revealed porous low density framework of nano C-γ-alumina (fig. 5) that comprised small spherical shaped nanoparticles, fastened manifoldly in carbon rich agglomerated bunches of spherical particle stacks. In contrast, imaging of C-α-alumina (fig. 6) displayed rigid and platy asymmetrical surface morphology that almost contained triangular, rectangular and polyhedral nanoparticle stacks. Except the shapes, imaging also illustrates huge variations in particles size for both organometallic specimens, ranging from ~500nm to ~26nm for C-γ-alumina, and from ~500nm to ~84nm for C-α-alumina nanoparticles respectively. The broad variations in size range obtained for both C-γ/α-alumina and rough surface morphology visualized only in C-α-alumina were pre-considered products of exothermic decomposition that often emerged in highly uncontrolled environment (elevated temperature). Imaging apparently proved that, turmeric molecules were not only capable to target a particular topology in bulk but also had significant impact to control texture and geometry of particles at nanoscale results in; homologous spherical shaped nanoparticles of C-γ-alumina.

ACTIVATION IN NANO C-γ-ALUMINA

Assay preparation for measurement of antimicrobial susceptibility

To determine reactive property, antimicrobial susceptibility of organometallic aluminates was examined against pathogenic bacterial strain *Acinetobactor* sp. (Gram-negative) by following standard CLSI (formerly, NCCLS) protocol [29]. *In-vitro* agar cup diffusion [30] method was adopted for quantitative estimation of minimal inhibitory concentration (MIC) of susceptible specimens. 85mm in diameter Mueller-Hinton [31] dish with depth of 4mm agar broth was used to provide proteins and other nutrients to culture a

confluent growth of bacterial organism. Inoculum of bacterial strain was prepared by suspending 48 hours old bacterial colonies in 1ml of sterilize saline water. Density of inoculum suspension was adjusted till the visible turbidity of suspension matched with 0.5Mc-Farland [32] standard. 100µl of bacterial inoculum was then pipette onto the surface of agar dish and streaked uniformly by a sterilize cotton swab. To prevent rapid agglomeration of nanoparticles and/or to obtain faithful diffusion, each participating specimens (except water) were dispersed ultrasonically (in ratio of 1mg/ml) in non-volatile, inert polydimethylsiloxane (>η, negative control) that remained diluted up to ~16 hours. Intimate contact for diffusion was provided by five 10mm cylindrical cups, which were ditched on agar surface by a sterilized borer. First cup was filled with 200µl of sterilize distilled water (negative control). Second cup was filled with 200µl of reference antibiotic Ofloxacin (Cipla, positive control). Third cup was filled with 200µl of an additional reference powder of pure alumina (Sigma-Aldrich). Fourth and fifth cups were filled with 200µl of as-synthesized organometallic nanoparticles of C-γ-alumina and transformed C-α-alumina respectively. To measure zones of inhibition, infected dish was then incubated on temperature 37°C in air for 24 hours.

Assay preparation for measurement of total dissolved solids (TDS) in water

To measure adsorptive property of C-γ-alumina nanoparticles present work dealt with *ex-situ* remediation of river water (Varuna-India) by continuous flow adsorption method. A qualitative measurement of dissolved ionized solids like minerals, salts and heavy metals ions in river water was obtained by conventional TDS (total dissolved solid) apparatus (Aqua Pro API-HM). For this purpose a 10cm glass column with diameter 2cm was prepared by following standard chromatographic column [33] procedure and packed with 4gm of C-γ-alumina nanoparticles to obtain a bed height of 1.5cm. Powder bed of nanoparticles in bottom of column was sealed by glass wool.

After a pre-determined time lapsed in incubator, minimal inhibitory concentration (MIC) of susceptible specimens yields a circular zone of inhibition (fig. 7a) in the immediate area around the cups for the given concentration. The zones of inhibition were measured as the widest diameter (mm) from the edges of the last visible colonies of bacterial culture. As per obtained results (Table. 1) negligible sign of inhibition zones or activities were displayed by pure

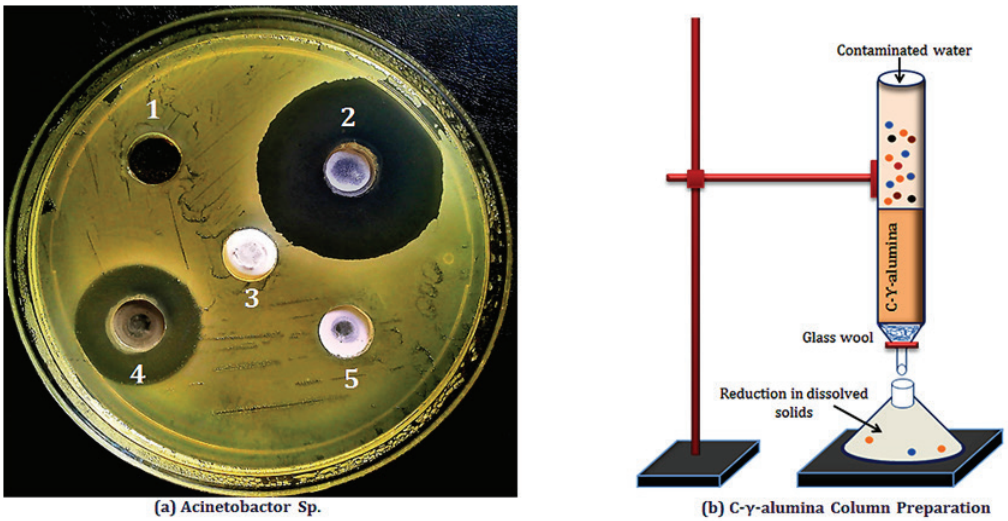

Figure 7. (a) MIC diameters of susceptible antibiotic Ofloxacin (cup 2) and C-γ-alumina (cup 4) formed against *Acinetobactor* sp., and C-γ-alumina column preparation for measurement of TDS in river water.

Pathogen	Specimen	Zone of inhibition (mm)	Equivalent MIC breakpoint (mg/ml)		
			Resistant	Intermediate	Susceptible
Acinetobactor	Ofloxacin	35	<28mm	39-33mm	>33mm
	Pure alumina	-	-	-	-
	C-γ-alumina	24	<18mm	19-22mm	>22mm
	C-α-alumina	-	-	-	-

Table 1. Susceptibility performance and equivalent MIC breakpoint of participating specimens

alumina (cup 3) and transformed C-α-alumina (cup 5) indicates; both specimens were inert and failed to interact chemically with the vital components of bacterial organism. Beside this, nanoparticles of C-γ-alumina significantly competed with reference antibiotic (cup 2) and secured a mild 24mm diameter zone of inhibition around the cup-4. This notable bactericidal property of C-γ-alumina further exposed its degree of resistivity against the bacterial growth and probably emerged due to the congenital cytotoxicity, intrinsically produced by γ-nanoparticles (catalytic) together with its alkaloid carbon derivatives (Phenol, phenyl and cyanide-nitrile). Toxicity of cyanide-nitrile compound was thought to generate mutation through apoptosis (cell death) [34], nourished parallel by well-known germicidal-antiseptic properties of phenol and phenyl groups [35]. Furthermore, during TDS measurement, the filtered 100ml of river water through C-γ-alumina column (fig 7b) indicates significant reductions in average concentration of total dissolved solids form 748.13ppm to 496.02ppm. The observed pH value of river water also decreased from 8.3 to 6.2 on pH scale. Adsorption of dissolved solids along with reduction in pH level further signified the binding efficacy of alkaloid carbon derivatives (functional groups) in form of active metal ligands that empowered organometallic C-γ-alumina to interact chemically with surrounding environment.

SUMMARY:

The overall experimental study inferred following confirmative conclusions;

- Thermal decomposition through solution combustion is a convenient way to introduce carbon in crystal lattice of dissimilar electronegative elements.
- 'Heat assisted covalent-ionic self-assembly' of carbon with inorganic oxide is possible in bulk volume.
- Turmeric molecules have formative self-assembling properties.
- 'Spherical shaped' C-γ-alumina nanoparticles confirmed the ability of carbon (turmeric transformed) to control geometry and texture of particles at nanoscale.
- The combination of high mechanical and physical properties of alumina together with reactive and adsorptive properties of turmeric in its respective carbon form (alkaloid functional groups) confirmed the hybrid characteristics of both parent materials in C-γ-alumina.
- Low temperature synthesis (700°C) of thermodynamically stable alpha alumina is feasible by hexamine propellant.

Fabrication of alumina "supermolecules" has fulfilled the aim of this work. Enhanced biochemical properties with comprehensive functioning, nanosized organometallic frameworks, hybrid physical and chemical state may help alumina to regain its lost identity as biomaterial.

ACKNOWLEDGEMENT

Authors oblige to acknowledge their sincere sense of gratitude to the individuals belongs to Department of microbiology IMS-BHU.

REFERENCES :

[1].Thamaraiselvi, T., and Rajeswari, S. (2004) Biological evaluation of bioceramic materials. Trends Biomater. Artif Organs, 18(1), 9-17.

[2].Gieske, J., and Barsch, G. (1967) Pressure dependence of the elastic constants of single crystalline aluminum oxide. Physica Status Solidi, 29, 121-131. http://dx.doi.org/10.1002/pssb.19680290113

[3].Park, B.J., and Bronzino, D.J. (2002) Biomaterials-Principal and Applications. CRC Press LLC, 23-25. ISBN; 0-8493-1491-7

[4].Burke, J., and Doremus, H.R. (1971) Static fatigue in glasses and alumina. Materials Sci. Res, 5, 435–444.

[5].Razali, A.W., Sreenivasan, V., and Goldys, E. (2014) Large scale production and characterization of biocompatible colloidal nanoalumina. Langmuir, 30(50), 15091-15101. http://dx.doi.org/10.1021/la5042629

[6].Rahman, S.H., Choudhury, D., and Osman, N.A. (2013) In-vivo and In-vitro outcomes of alumina, zirconia and their composited ceramic-on-ceramic hip joints. J Ceram Society Japan, 121(1412), 382-387. http://dx.doi.org/10.2109/jcersj2.121.382

[7].Navarro, M., and Michiardi, A. (2008) Biomaterials in orthopedics. J Royal Society Interface, 5(27), 1137-1143. http://dx.doi.org/10.1098/rsif.2008.0151

[8].Harry. (2006) Alumina in homeopathy an open homeo-encyclopedia project. Available on http://www.homeopathyandmore.com/fourm/viewtopic.php?t=100

[9].Kasi, K.A., Kasi, K.J., Hasan, M., and Pankiew, A. (2012) Fabrication of low cost anodic aluminum oxide tubular membrane and their application in hemodialysis. Advanced Materials Research Switzerland, 550(553), 2040-2045. http://dx.doi.org/10.4028/www.scientific.net/AMR.550-553.2040

[10].Roualdes, O., Duclos, M.E., Frappart, L., and Hartmann, D.J. (2010) In-vitro and In-vivo evaluation of an alumina-zircona composite for arthoplasty applications. Biomaterials, 31, 2043-2054. http://dx.doi.org/10.1016/j.biomaterials.2009.11.107

[11].Poinern, G., Fawcett, D., Brundavanam, R., and Jiang, Z. (2010) Nanoengineering a Biocompatible Inorganic Scaffold for Skin Wound Healing. Journal of Biomedical Nanotechnology, 6, 497-510. http://dx.doi.org/10.1166/jbn.2010.1148

[12].Stanford, M.C., and Keller, J.C. (1991) Osseointegration and matrix production at the implant surface. CRC Critical Review Oral Biol Med, 2(1), 83-101.

[13].Bohlar, M., Mochida, Y., Plank, H., and Salzer, M. (2002) Wear debris from two different alumina on alumina total hip arthoplasties. J. Bone Joint Surg. (Br), 82(B6), 901-909.

[14].Groot, D.K. (1988) Effect of porosity and physicochemical properties on the stability, resorption and strength of calcium phosphate ceramics. Annual N Y Academic Science, 523, 227-233.

[15].Kong, Y.M., Bae, J.C., Lee, H.S., Kim, W.H., and Kim E.H, (2005) Improvement in biocompatibility of ZrO2-Al2O3 nano-composite by addition of HA. Biomaterials, 26, 509-517. http://dx.doi.org/10.1016/j.biomaterials.2004.02.061

[16].Hassan, S.F., and Gupta, M. (2004) Development of high-performance magnesium nanocomposites using solidification processing route. Mater. Sci. Technol, 20, 1383-1388.

[17].Levin, I. (1998) Metastable alumina polymorphs crystal structures and transition sequences. J American Ceram Society, 81(8), 1966-2012.

[18].Wyckoff, W.R. (1951) Crystal structures. Interscience New York, 2(2), 13-14. http://dx.doi.org/10.1002/ange.19530650914

[19].Cava, S. (2007) Structural characterization of phase transition of

Alumina. Materials Chemistry and Physics, 103, 394-399. http://dx.doi.org/10.1016/j.matchemphys.2007.02.046
[20].Gyo, Lee.W. (2013) Phase transition characteristics of flame synthesized gamma Al2O3 nanoparticles with heat treatment. International Journal of Chemical. Materials Science and Engineering, 7(9), 67-70.
[21].Jager, D., and Prashanti, T. (2010) Turmeric, the ayurvedic spice of life. Pioneer Imprints, 2, 129
[22].Dujardin, E., Hsin, B.L., Chris, R.C., and Mann, S. (2001) DNA-driven self-assembly of gold nanorods. Chemical Communication, 1264-1265. http://dx.doi.org/10.1039/B102319P
[23].McGlynn, E.S., Mulder, W.D., Shepard, M.E., and Peters, J. (2009) Hydrogenase cluster biosynthesis: organometallic chemistry nature's way. RSC Dalton Transactions, 22, 4274-4285. http://dx.doi.org/10.1039/b821432h
[24].Smith, W.D. (1999) The strength of carbon-carbon bonds in metal alkyls. J organomet chem Elsevier Science, 585, 150-153. http://dx.doi.org/10.1016/S0022-328X(99)00207-7
[25].Jensen, B.W. (1996) Electronegativity from Avogadro to Pauling: Origins of the electronegativity concept. Journal of chemical education, 73(1), 11-21. http://dx.doi.org/10.1021/ed1011822
[26].Coates, J. (2000) Interpretation of Infrared spectra: A practical approach. Encyclopedia of analytical chemistry. R. A. Meyers Ed. John Wiley, 10815-10837.
[27].Characteristics IR absorption frequencies of organic functional groups. Available on http://www2.ups.edu/faculty/hanson/spectroscopy/IR/IRfrequencies.html
[28].Shouwen, S., Sitepu, H., and Alabedi, G. (2010) Use of XRD and XRF technique to determine the chemical composition and crystallite size of metal matrix composite materials. Saudi Aramco journal of technology, 50-55.
[29].Karatuna, O., (2008) Quality assurance in antimicrobial susceptibility testing. Latest Research in Quality Control-INTECH, 19. http://dx.doi.org/10.5772/51998
[30].Alli, A.I., Ehinmidu, J.O and Ibrahim, K.E. (2011) Preliminary phytochemical screening and antimicrobial activities of some medicinal plants used in Ebiraland. Bayero Journal of Pure and Applied Sciences, 4(1), 10-16. http://dx.doi.org/10.4314/bajopas.v4i1.2
[31].Boyanova, L., Gergova, G., Nikolov, R., Lazarova, E., and Katsarov, N. (2005) Activity of Bulgarian Propolis against Helicobacter pylori strains in-vitro by agar well diffusion, agar dilution, and disc diffusion methods. Journal of Medical Microbiology, 54, 481-483. http://dx.doi.org/10.1099/jmm.0.45880-0
[32].Wotton, M. (2013) BSAC Methods for Antimicrobial Susceptibility Testing. British Society for Antimicrobial Chemotherapy, 13, 1-87.
[33].Sharma, Y., Srivastava, V., and Mukherjee, A. (2010) Synthesis and application of nano-Al2O3 powder for the reclamation of hexavalent chromium from aqueous solution. J Chem Eng Data, 55, 2390-2398. http://dx.doi.org/10.1021/je900822j
[34].Debord, S., Bourdin, G., Stoian, A., Bayle, F., Leray, V., and Richard, C.J. (2013) Pink skin, urine and effluent fluid after cyanide poisoning. J Medical Disord, 1, 1-3. http://dx.doi.org/10.7243/2053-3659-1-3
[35].Marvibaigi, M., Amini, N., Supriyanto, E., Jamil, S., and Majid, F. (2014) Total phenolic content, antioxidant and antibacterial properties of Scurrula ferruginea extracts. Jurnal Teknologi, 70(5), 65-72.

Cite this article as :

Vishnu Prabhakar, Rupesh Kumar, Aditi. Synthesis and Characterization of Turmeric Powered Bio-Significant 'Organometallic Aluminates'. Asian Journal of Biomedical and Pharmaceutical Sciences. 5(41), 2015: 7-14.